Effect of Cryogenic and Electrolytic passivation treatment on Wear Resistance of M2 High-Speed Steel

Zhi Chen
Yangwei Zhang (zyw170126@163.com)
TYUST: Taiyuan University of Science and Technology
Xianguo Yan
Jiale Li
Fan Li

Research Article

Keywords: M2 high speed steel, cryogenic treatments, electrolytic passivation treatment, wear resistance

Posted Date: September 2nd, 2022

DOI: https://doi.org/10.21203/rs.3.rs-1998851/v1

Version of Record: A version of this preprint was published at The International Journal of Advanced Manufacturing Technology on May 31st, 2023. See the published version at https://doi.org/10.1007/s00170-023-11639-z.

Abstract

Through cryogenic treatment and electrolytic passivation treatment of M2 high-speed steel(HSS), the effect of electrolytic passivation process parameters on the life of M2 HSS taps and the combined effect of cryogenic treatment and electrolytic passivation treatment on the wear resistance of the M2 HSS were investigated by using a scanning electron microscope (SEM) and energy dispersive spectrometer (EDS). The results show that the life of M2 HSS tap after electrolytic passivation treatment increases most significantly under the theoretical edge radius, the functional relationship between the charge consumption (y) and the tap edge radius (x) is as follows: y = 8.135x-48.842. The wear resistance of the sample after cryogenic and electrolytic passivation treatment is the highest, which is 1.52 times higher than those of the traditional heat treatment sample. This is due to the increase of the number of carbides on the surface of the specimens after cryogenic treatment, the distribution and size of carbides are relatively uniform, the average size of carbides is reduced by 60.4%. There is a carbon layer on the surface of the sample after passivation, which can effectively improve the wear condition. The size and number of carbides in the surface layer of the sample remain unchanged after passivation treatment, indicating that cryogenic treatment plays a key role in the performance of the material.

1 Introduction

As a high alloy tool with high hardness, HSS is widely used in various sophisticated tools such as taps, drill bits, and broach cutters[1].

Cryogenic treatment is an extension of the heat treatment process, which has also been shown to significantly improve the material properties of HSS cutting tools[2]. After cryogenic treatment, HSS tools exhibit superior wear resistance and dimensional stability[5]. The increase of cryogenic technology in the industrial field has greatly extended the HSS service life[8]. The cryogenic treatment is an effective method to improve the wear resistance of M2 steel, and studies show that 77k cryogenic temperature and extension of cold holding time to 24h can significantly increase its wear resistance [9]. The service life of the M2 HSS drill is increased by 126% after being immersed in liquid nitrogen for 24 hours and then tempered at 473K. The cryogenic treatment not only promotes the transformation of retained austenite to martensite but also uniformly precipitates elliptical carbide particles, which enhances the service life of high-speed steel tools[10].

Since micro-defects such as burrs and openings often exist in HHS tools such as taps after sharpening, electrolytic passivation is a common solution to a series of problems such as micro-cracks, uneven surface, and unstable. cutting performance caused by sharp edges. The edge of the tap is smoother after electrolytic passivation and the roughness of the rake face of the cutting tool is significantly reduced, which can improve the service life of HSS taps [11]. The feasibility of the electrolytic passivation treatment and carried out the electrolytic passivation treatment for cemented carbide cutting tools, to eliminate the micro-defects of the cutting tools and improve the surface quality of the workpiece[12]. The changes of tangential force, radial force, and friction force in cutting titanium alloy at different cutting

edge radius and cutting speeds, and found that the friction force when cutting titanium alloy is not only affected by the cutting speed but also related to the value of cutting edge radius of the tool[13].

However, the relationship between electrolytic passivation process parameters and the service life of HSS taps and the mechanism of the combined effect of electrolytic passivation and cryogenic treatment on the wear resistance of HSS has not been studied in depth. Therefore, the electrolytic passivation treatment of M2 HSS taps is used to establish the relationship between the electrolytic passivation process parameters and tap life, optimize the electrolytic passivation process parameters, and perform electrolytic passivation and cryogenic treatment on M2 HSS to reveal the evolution mechanism and organization of the wear resistance of HSS by electrolytic passivation and cryogenic treatment, and to provide guidance for industrial applications.

2. Effect Of Electrolytic Passivation Process Parameters On The Life Of M2 Hss Taps

2.1 materials and test specimens

For the experimental work, M2 high-speed steel was used. This steel had the following chemical composition (in wt.%): 0.82% C, 0.20% Si, 0.13% Mn, 0.3% Ni, 0.001% S, 4.10% Cr, 4.50% Mo, 2.10% V, and 6.10% W. The mechanical tap with manufacturing standard of GB966–67 was selected with the specification of M8 × 1.25, the precision of H2, the front angle of 8.69°, the back angle of 4.96°.

A TYESM-15 electrolysis equipment independently developed by the laboratory with a 500 mm cell capacity was used for passivation with the voltage and current ratings of 220 V and 0–10 A, respectively, cutting tool diameters of 3-12mm, and spindle speeds of 0-120r/min. The sample is clamped in the electrolytic anode and phosphoric acid solution is used as an electrolyte. During electrolytic passivation, the whole process is automatically controlled by the program. After the electrolysis passivation test, the sample was neutralized in 5% Na_2CO_3 solution, and then cleaned in water.

2.2 Theoretical dimensions of tool edge radius

Electrolytic passivation treatment can eliminate the unevenness of the tap edge and improve the tap edge radius to increase the life of the tap. The relationship between the theoretical edge radius size of the tap and the tool angle is shown in Fig. 1[14].

where r is the edge radius, γ_0 is the front angle, and α_0 is the back angle. The unevenness of the cutting edge applicable to most cutting tools ranges from 0.01mm to 0.05mm, the edge unevenness takes the minimum value of 0.01 and the maximum value of 0.05 accordingly, so the range of edge radius is 0.016mm-0.060mm. Given that the tap is a small precision tool with multiple cutting edges, the cutting part of the cutting edge is short, the radius of the cutting edge will be blunted if the reference is based on the standard of other tools, the value of the edge radius of the tap should be smaller, and the value of the blunt radius is 0.016mm.

2.3 Relationship between electrolytic passivation process parameters and tap edge radius

The main adjustable. electrolytic parameters of the electrolytic passivation equipment used in this experiment are electrolytic power consumption, in Coulomb (c). The relationship between coulomb C and the tap edge radius is established. The basic test environment is: the electrolytic power supply is 12V DC high-frequency pulse power supply, the spindle speed is 120rpm, the electrolyte is the phosphoric acid solution, and the electrolyte temperature is 25 ℃. Six groups of taps with an electrolytic power consumption of 100C, 200C, 300C, 400C, 500C, and 600C were tested for passivation, with three taps in each group.

After passivation, the tap edge radius of each group was measured and averaged on SEM (JSM-6510, JEOL, Tokyo, Japan), and the values of tap edge radius with different energizing charges are shown in Table 1, the passivation effect of different electrolytic power consumption on the tap edge is shown in Fig. 2. As can be seen from Fig. 2, after electrolytic passivation, the tap presents different degrees of blunt and the edges become round. At the same time, due to the fast discharge rare of the tip of the tap, the dissolution speed is also fast, making the surface flat. When the energized charge is high, the surface will be dissolved to produce very many small

pits, which is very beneficial for the storage of cutting fluid.

Table 1
Values of edge radius of the taps with different energizing charges

Charge quantity(C)	1st tooth edge radius(μm)	2st tooth edge radius(μm)	3st tooth edge radius(μm)	Average value(μm)
15	4.85	4.46	4.19	4.50
30	9.01	9.85	9.67	9.51
50	10.11	9.55	10.53	10.06
75	16.77	17.39	17.31	17.16
100	20.83	19.68	19.91	20.14
150	27.70	26.48	26.56	26.91
200	33.90	34.29	33.53	33.90
300	40.86	40.32	42.53	41.24
400	54.43	55.11	53.91	54.48
500	66.25	64.06	67.28	65.86

A scatter plot of electrolytic passivation power consumption versus tap edge radius was plotted and fitted as a function by MATLAB software, as shown in Fig. 3. The function between the charge quantity (y) and the tap edge radius (x) is y = 8.135x – 48.842.

2.4 Effect of edge passivation on life of M2 HSS tap

According to the function, it can be seen that the theoretical edge radius of this type of tap is 16μm, and the corresponding electrolysis parameters are near 75 C. Therefore, the electrolysis parameters for this test are 0C, 50C, 75C, 100C, 150C, and 200C, of which 0C is the comparison group without passivation.

The six groups of taps were tapped after the above electrolytic passivation treatment to study the relationship between the electrolytic passivation process parameters and the life of HSS taps. WMD0912 Wanmuchun brand tapping machine was used in this experiment. The tapping cutting speed was 10.807 m / min (spindle speed 430 r / min). The processed material was H13 steel, processing method selected through-hole processing, bottom hole diameter of 6.8 mm, tap failure criteria by measuring maximum flank face wear$VB_{\max}$(The national standard stipulates that the blunt standard for M8 taps is 0.45mm.)[15]. As shown in Fig. 4, the maximum wear values of the taps' flank face were recorded for six groups of taps when machining 10, 20, 40, and 60 holes, respectively. From this diagram, it can be seen that the overall wear trend of the six groups of taps is roughly in line with the typical three stages of flank face wear: initial wear stage, normal wear stage, and rapid wear stage.

In the initial wear stage, the wear rate of the unpassivated tap is the fastest, and the back tool surface presents the form of groove wear. After machining 10 holes, the wear has reached the maximum among the 6 groups of taps, while the other groups of passivated taps all wear slower than the unpassivated taps. The reason for the faster wear rate of the 200C passivation taps is due to the instability of the cutting process and the vibration of the spindle caused by a large amount of passivation and the blunt edge, which aggravates the wear of the tap.

In the normal wear stage, due to the defects of the unpassivated taps themselves, the whole life cycle is short and the wear rate is very fast. The normal wear phase is not obvious and the effective time of work is very short, and it also indicates that the quality of the unpassivated taps for machining holes is not stable. The 150C passivated tap has reached the wear standard before 40 holes due to the cutting heat and poor chip removal during continuous machining.

The rapid wear stage should be avoided as much as possible. The unpassivated tap has already reached the rapid wear stage, and there are abnormal failure forms such as large-scale chipping. Due to the extension of the normal wear stage of the 50C, 75C, and 100C passive taps, the rapid wear stage is not obvious during the effective working period, which largely avoids the abnormal failure mode. The wear rate of the passivated taps at this phase is also significantly lower than that of the non-passivated taps.

Based on the above experimental results and analysis, when the electrolytic passivation charge is 75 C, that is, the tap edge radius is about 17 μm, the life of the tap has the highest improvement. the wear resistance is better at the initial stage of wear, the normal wear stage is prolonged, the effective working

time is increased, and the working efficiency is improved. To a certain extent, the rapid wear stage is avoided, and the abnormal wear form is greatly alleviated. The processing is stable and reliable, and the passivation effect is the best.

3. Effect Of Cryogenic Treatment And Electrolytic Passivation On Wear Resistance Of M2 Material

3.1 Sample materials and preparation

In order to study the effect of cryogenic treatment and electrolytic passivation on the wear resistance of M2 HSS, two types of samples were selected. The first type dimension was $\varphi 40 \times 10 mm^3$. The size of the second type was $5 \times 5 \times 10 mm^3$, cut from the first type after the experiment.

3.2 Heat treatment and cryogenic treatment process

According to the summary of the cryogenic test at the early stage, it is considered that the toughness and wears resistance can be well balanced by the cryogenic treatment before tempering, which aims to improve the service life and cutting performance of HSS taps[7]. In this experiment, the quenching and tempering treatments were conducted in a vacuum furnace (VHQ-122l-06, Shenyang Jayu vacuum technology Co.Ltd, Shenyang, China). To balance the macro-properties, the quenching temperature is set at 1483K. Cryogenic treatment was conducted by our homemade cryogenic equipment (TYKD – 1, Taiyuan University of Technology and Science, Taiyuan, China). The cryogenic temperature was set at 118K for 360min, which cooling rate is 1 K/min. Tempering temperature is selected as 833K. According to the traditional heat treatment process of HSS, there were three times conventional tempering treatments, which the heat preservation was carried out for 60minutes. All details were shown in Fig. 5.

3.3 Electrolytic passivation treatment process

The electrolytic passivation treatment was performed in an electrolytic passivation apparatus (TYESM-15). The sample under test was clamped in the electrolytic anode, and the power consumption, current, and voltage were set to 1000 C, 10 A, and 10 V, respectively.

3.4 The experimental scheme of M2 HSS material

Based on the experimental results previously published by the research group, the experimental schemes include the QT group, the QTP group, the QCT group and the QCTP group[17]. The experimental scheme is shown in Table 2, and there are 3 samples in each group. The schematic diagram of cryogenic treatment and electrolytic passivation is shown in Fig. 6.

Table 2
Heat treatment and cryogenic treatment and electrolytic passivation treatment process

Groups	Quenching Temperature(K)	Cryogenic Temperature(K)	Cryogenic times	Tempering Temperature(K)	Electrolytic passivation
QT	1483	293	0	833	N
QTP	1483	293	0	833	Y
QCT	1483	118	3	833	N
QCTP	1483	118	3	833	Y

3.5 Wear test

According to the experimental scheme, the grinding process was finished on the "M7130" surface grinding machine (M7130, Beijing North First machine tool Co. Ltd, Beijing, China) after the tempering process, the surface roughness was under 0.8μm. Samples were finished on the polishing machine (PG -1, Chinese Nanjing Lianchuang analytic instrument Co. Ltd, Nanjing, China) after grinding process. The samples were put into an ultrasonic cleaning machine to clean with acetone solution before the wear test. Then, there were three samples in each group, which need to be strengthened by electrolytic strengthening treatments. Tapping can be simply regarded as the friction pair formed by tap and workpieces. The purpose of the wear test is to simulate the wear condition and explain the impact of wear conditions on the material properties, which is to select the optimal process and process parameters[19]. According to tapping process simulation by a research group in an earlier stage, the tapping highest temperatures could be 773K. The test parameters are selected according to the working conditions of high-speed steel tap tapping[22]. A ball-on-disc high-temperature (T = 773 K) wear test unit (HT-1000, Lanzhou Zhongke Kaihua technology development Co. Ltd, Lanzhou, China) with Si3N4 balls (dia: 5mm, 78HRC) was used for the wear tests under a load of 19.8N, a linear velocity of 120 m/min., and a turning radius of 7.5 mm. The tests were run for 60 min. for a total distance of 7200 m.

When the temperature was reduced to room temperature after the wear test, the wear volume test was finished on a surface performance comprehensive tester (CFT- , Lanzhou Zhongke Kaihua technology development Co. Ltd, Lanzhou, China), each sample was measured 5 times in different locations.

3.6 Microscopic analysis

After the macro-properties test, the samples were cut into the second type. The second type has two types of samples, which were samples including wear scars (WS) and samples without wear scars (WWS).

The observation surface of WWS samples was polished with abrasive paper to make the surface free from scratches. Then the PG-1 metallographic polishing machine was used for polishing. Chromium trioxide was used as the polishing powder, which was polished to the bright surface. The metallographic corrosion was carried out on the observation surface with an 8% nitric acid alcohol solution. Finally, a

scanning electron microscope (SEM) and an energy dispersive spectrometer (EDS) were used to observe the carbides precipitation status of samples.

The WS samples were cleaned in acetone solution at room temperature for 30min. The surface morphology of wear scars was observed with an optical microscope to ensure that they were clean. The wear scars were observed by SEM and the wear mechanism was speculated by EDS.

4 Results And Discussion

4.1 Analysis of wear test results

4. 1.1 The influence in different processes on friction coefficient

To make the test results more impartial, there are three samples in each group and the final friction coefficient consists of the average of the three friction coefficients at each collection time point. Figure 7 shows the variation of the friction coefficient for four groups of specimens with a wear time of 60 min.

It can be seen from the Fig. that:

(1) The friction coefficient before and after cryogenic was compared. Comparing the friction coefficient curves of the QT group and QCT group, the friction coefficient of QCT group specimens after deep cooling treatment is lower than that of QT group specimens without deep cooling treatment. The friction coefficient of the QT group had a periodic trend of repeated cycle rise and sudden drop, fluctuating between 0.65 and 0.71. There was no significant difference in the time required for the two groups of samples in the pre-grinding stage, which was about 3 ~ 4 min. After entering the normal wear stage, the friction coefficient of the QCT group after cryogenic treatment fluctuated slightly, and the final friction coefficient decreased to about 0.55.

(2) Comparison of friction coefficients before and after electrification. Comparing the friction coefficient curves of the QT group and QTP group, the friction coefficient of specimens in the QTP group after electrolytic passivation is lower than that of specimens in the QT group without electrolytic passivation. In the early stage of friction, the friction coefficient of the QTP group after electrolytic passivation was larger than that of the QCT group after cryogenic treatment. However, after 30 min, the friction coefficient of the QTP group fluctuated up and down in the friction coefficient curve of the QCT group, and the average friction coefficient of the QTP group was 0.124 lower than that of the QT group.

(3) For the friction coefficient curve of the QCTP group, it was slightly higher than that of the QTP group and the QCT group at the first 30 min, but after a small range of shock for 20 min, it was stabilized near 0.5 at the late stage of wear, and the average friction coefficient of QCTP group was reduced by 0.151 compared with that of QT group.

(4) By comparing the friction coefficient curves of the four groups, it can be seen that both cryogenic treatment and electrolytic passivation can effectively reduce the friction coefficient value during high-

temperature wear. The friction coefficient value of the specimen after cryogenic treatment has a significant tendency to decrease, and the specimen will have a black carbon layer on the surface of the specimen after electrolytic passivation treatment, as shown in Fig. 8. It is preliminarily judged that the reason for the appearance of the carbon layer is that during the electrolytic passivation process, the sample was used as an anode. After the metal atoms on the surface of the sample lost electrons and became metal cations into the solution, the residual carbon atoms on the surface of the sample had a certain lubrication effect, so the friction coefficient of the sample after electrolytic passivation treatment could be effectively reduced. Cryogenic treatment and electrolytic passivation treatment are superimposed for better wear resistance, but the decisive role is played by the cryogenic treatment, and electrolytic passivation cannot significantly expand this advantage.

4.1.2 The influence in different processes on relative wear resistance

Relative wear resistance$E = W_A/W_B$ refers to the ratio of wear amount of two different materials under the same wear condition. The wear amount of one material sample is taken as the standard.W_A is the Volume loss of standard samples, W_B is the volume loss of the target samples[23].

Each group's wear volumes were measured in CFT - material surface performance comprehensive test instrument. Table 3 show the changes of relative wear resistance of different processes.

Table 3
Relative wear rate under different processes.

Different process	QT	QTP	QCT	QCTP
Relative wear rate	1	1.09	1.34	1.52

It can be seen from Table 10 that the relative wear resistance of the QTP group, the QCT group, the QCTP group, and the QT group was 1.09, 1.34, and 1.52 times higher than that of the QT group, respectively. It was further verified that both electrolytic passivation and cryogenic treatment can improve the wear resistance of M2 HSS, but the decisive role is played by the cryogenic treatment.

4.2 Wear scar analysis

To illustrate that cryogenic treatment and electrolytic passivation treatments can effectively improve the wear resistance of M2 HSS, wear scars were observed under an optical microscope.

ImageJ software was used for image processing of the wear scars. Table 4 shows the area of wear scars (AWS), the average size of wear scars (ASWS), and the percentage of wear scars sizes (PWSS). Figure 9 shows the SEM images of the wear scars of the four groups of samples after high-temperature wear and the corresponding element contents measured by EDS.

It can be seen from Table 9 that the surface wear of the QT group sample is serious, with the largest ASWS, and the PWSS is 61.2%. After cryogenic treatment, the wear scar of the QCT group is significantly reduced, and the ASWS is relatively small, with the PWSS of 30%. After electrolytic passivation treatment, the ASWS of the QCP group can also be reduced by nearly 48%. It shows that cryogenic treatment and electrolytic passivation treatment can effectively alleviate the wear, and the QCTP group after cryogenic treatment and electrolytic passivation treatment has the best effect.

From Fig. 9 it can be seen that:

Figure 9(a) (b) show the SEM and the EDS diagrams of the wear scars of the QT group samples. It can be seen from Fig. 9(a) that this group of samples is the most seriously worn one of the four groups of samples, which is reflected in the large area of dark black plow mark trauma morphology. The dark black oxidation marks are continuous and large area, and many spherical particle debris are attached to the wear surface, and the plowing material is stacked on both sides of the groove in a large amount and accompanied by the traces of material flaking off in a whole piece. From Fig. 9(b), it can be seen that the surface layer of the specimen contains a high content of oxygen and tungsten elements, indicating the presence of oxidative wear on the surface layer as well as the exposure of the inner matrix after the damage by adhesive wear. Therefore, the wear mechanism of this group is mainly abrasive wear and adhesive wear, and the degree of oxidation wear is generally serious at 773K. In comparison, the most typical wear forms in this group are still abrasive wear and adhesive wear.

Figure 9(c), (d) show the SEM and the EDS diagrams of the wear scars of the QCT group samples. It can be seen from Fig. 9(c) that after cryogenic treatment, the surface wear morphology of the sample was improved compared with that of the QT group. The main manifestations were that the groove wear traces were less and deeper, the furrow area was small and incoherent, and a small amount of soft material had obvious traces of tearing down the whole oxide layer. As can be seen from Fig. 9(d), the higher content of carbon elements in this group of specimens indicates that more carbide precipitates in the surface layer after cryogenic treatment, which helps to reduce the degree of wear damage. The main wear mechanisms are oxidation wear and adhesive wear, as well as lighter abrasive wear.

Figure 9(e), (f) are the SEM and EDS images of the wear scars of the QTP group. Figure 9(e), (f) are the SEM and EDS images of the wear scars of the QTP group. The results show that after electrolytic passivation, the furrows on the surface of the sample are lighter, and there are a small amount of traces of the oxide layer peeling off on the surface, and the content of the C element in the surface is 3 times that of the unpassivated sample. It shows that after electrolytic passivation, the surface metal atoms become free metal ions under the action of electrolyte, and the remaining C atoms in the surface increase the lubrication effect of friction. The main wear mechanisms are oxidation wear and slight abrasive wear and adhesive wear.

Figure 9(g), (h) are the SEM and EDS diagrams of the wear scars of the QCTP group samples, from which it can be seen that the group specimens have more traces of oxide layer peeling off after deep cooling and electrolytic passivation treatment, and the content of oxygen and iron elements are higher, indicating

that after the oxide peels off from the surface layer through fatigue wear, the presence of abrasive chips between the two wear surfaces plays a weak role in reducing wear and effectively relieves wear. Therefore, it can effectively reduce the friction coefficient in the late stage of frictional wear. At the same time, the content of the C element increased from 8.7% of the QT group to 18.9%, which also played a role in lubricating the friction surface. The main wear mechanism is oxidation wear.

Table 4
The calculation of the wear scar.

Treatment	AWS (μm^2)	ASWS (μm^2)	PWSS (%)
QT	624015.9	377.734	61.2
QCT	305472.3	76.064	30
QCP	324684.6	77.050	31.2
QCTP	266779.1	62.100	26.2

4.3 Microstructure

In the past, the researches of HSS wear performance mainly focused on the different heat-treatment processes. Now, cryogenic treatment is generally recognized by the heat treatment field, which especially generates the greatest effect in the carbides precipitation of HSS[24]. The cryogenic treatment provides the driving force for transformation from residual austenite to martensites, which increases the number of fine martensite and reduces the rate of lattice distortion. The smaller the size of carbides is the better strengthening effect it generates. The carbides are divided into primary carbides (FC: size$> 5\mu m$) and secondary carbides (SC: size$\leqslant 5\mu m$). The size of the carbide is $1\backslash sim\ 5\mu m$, which is seen as the large secondary carbides (LSC). The size is$0.1\backslash sim\ 1\mu m$, which is seen as the small secondary carbides (SSC)[25]. The more secondary carbides there are, the better material properties will be. Figure 10 is the four group's carbide images taken by scanning electron microscopy (SEM) at 3000 times. The white matters in the pictures are carbides. We can count the number and size of carbide particles by ImageJ software, and the specific data were shown in Table 5.

Figure 10 intuitively shows the distribution of carbide particles. Many primary carbides are precipitated from liquid steel during the process of condensation, which is eutectic and hypereutectic carbides. Secondary carbides are precipitated from the solid matrix during heat treatment or other treatment processes. Therefore, it can be seen that the fine carbide is precipitated at the grain boundary and distributed on the matrix.

According to Fig. 10 and Table 4, we should pay attention to the proportion that the number of different type's carbides accounts for the total number. It can see clearly that the total number of the first group is much lower than the other three groups. Carbide distribution is very sparse. There are some segregation

phenomenons of carbide, and many matrices do not exist carbide. The proportion of primary carbides was 5.7%, large secondary carbides were 44.3%, and small secondary carbides were only 50%, which is far lower than the other three groups. The stacking of carbides will lead to the stress concentration of materials. Many primary carbides could not improve the performance of steel, which will waste alloy elements and reduce the utilization rate of alloy. The average size of carbide was as high as1.342, which is much higher than other groups.

As for the principle of cryogenic treatment leading to the precipitation of small secondary carbides, the mainstream believes that the transformation of carbides is activated by the cryogenic treatment in this field. The generation of tempered martensite is also accompanied by the precipitation of small carbides, and the release of energy improves the nucleation rate of carbides. The small secondary carbides present a spherical shape after cryogenic treatment. The total numbers of the second group carbide are 244. The carbide distribution and size are relatively uniform, which the primary carbide accounts for 0.8% of the total number, large secondary carbides account for 5.3%, and small secondary carbides account for 93.8%. The average size of the carbide is about 0.473, so wear resistance is relatively good than the fourth group. Small particles of dispersion carbide are distributed in the matrix and grain boundaries, and the dispersion is more uniform than the other three groups, which effectively improves the wear resistance of M2 HSS.

It can be seen from Fig. 10(c) and Fig. 10(d) that the size and number of carbides remain unchanged before and after passivation treatment, which indicates that the internal structure of the material will not change after electrolytic passivation treatment. Cryogenic treatment plays a key role in material performance.

Table 4
Carbide statistics of four groups of samples

Groups	FC	SSC	LSC	Sum	Mean value
QT	6	53	47	106	1.342
QCT	2	229	13	244	0.473
QTP	7	64	45	116	1.132
QCTP	3	216	22	241	0.532

5 Conclusions

The effect of electrolytic passivation process parameters on the life of M2 HSS taps and the combined effect of cryogenic treatment and electrolytic passivation treatment on the wear resistance of M2 HSS was investigated. Based on the results obtained in the present investigation assist to infer the following major conclusions:

(1) Through the electrolytic passivation treatment and tapping experiment of M2 HSS tap, it is concluded that the life of M2 high-speed steel tap after electrolytic passivation treatment is the most obvious under the theoretical tap edge radius, the function between the charge quantity (y) and the tap edge radius (x) is y = 8.135x-48.842. It can be used to guide industrial mass production, improve production efficiency and service life of tap tools.

(2) The surface of samples with electrolytic passivated appears a layer of graphite. Based on the property of lubrication of graphite, the wear resistance of samples with electrolytic strengthening was improved. The normal wear stage of the flank is effectively prolonged.

(3) The high-temperature wear forms of the traditional heat specimens are mainly abrasive wear and adhesive wear, while the high-temperature wear forms of the specimens after cryogenic treatment and electrolytic passivation treatment are mainly oxidation wear and slight adhesive wear.

(4) The wear resistance of cryogenically treated samples is better than that of non-cryogenic treated samples, which is due to the increase of secondary carbide content. Electrolytic passivation treatment can also improve the wear resistance of the sample, but after electrolytic passivation treatment, the internal structure of the material does not change, and cryogenic treatment plays a key role in material performance.

Declarations

Author contribution All authors contributed to the study conception and design. Material preparation and data collection were performed by Xianguo Yan, Jiale Li, and Fan Li. The data analysis was performed by Zhi Chen and Yangwei Zhang. The first draft of the manuscript was written by Zhi Chen and all authors commented on previous versions of the manuscript. All authors read and approved the final manuscript.

Funding Authors would like to thank the Natural Science Foundation of China (NSFC) (No. 51275333) for financial support.

Availability of data and material Not applicable.

Code availability Not applicable.

Declarations

Ethics approval Not applicable.

Consent to participate Not applicable.

Consent for publication Not applicable.

Competing interests The authors declare no competing interests.

References

1. Simranpreet Singh Gill, Jagdev Singh, Rupinder Singh et al (2012) Effect of Cryogenic Treatment on AISI M2 High Speed Steel: Metallurgical and Mechanical Characterization. Journal of Materials Engineering and Performance 21:1320-1326. doi:10.1007/s11665-011-0032-z
2. Niu Xuemei, Huang Yao, Yan, Xianguo et al (2021) Optimization of Cryogenic Treatment Parameters for the Minimum Residual Stress. Journal of Materials Engineering and Performance 12:1-10. doi:10.1007/S11665-021-06136-X
3. Jovičević-Klug Patricia, Jenko Monika, Jovičević-Klug Matic et al (2021) Effect of deep cryogenic treatment on surface chemistry and microstructure of selected high-speed steels. Applied Surface Science. doi:10.1016/J.APSUSC.2021.149257
4. Jun-wan LI, Lei-lei TANG, Shao-hong LI et al (2012) FEM simulation and experimental verification of temperature field and phase transformation in deep cryogenic treatment. Transactions of Nonferrous Metals Society of China 22:2421-2430. doi:10.1016/S1003-6326(11)61480-5
5. Zeju Weng, Kaixuan Gu, Kaikai Wang et al (2019) Effect of deep cryogenic treatment on the fracture toughness and wear resistance of WC-Co cemented carbides. International Journal of Refractory Metals and Hard Materials(C) 85:105059-105059. doi:10.1016/j.ijrmhm.2019.105059
6. Podgornik, B., Paulin, I., Zajec, B. et al (2016) Deep cryogenic treatment of tool steels. Journal of Materials Processing Technology 229:398–406. doi:10.1016/j.jmatprotec.2015.09.045
7. Yan, X.G., Li, D.Y. (2013) Effects of the sub-zero treatment condition on microstructure, mechanical behavior and wear resistance of W9Mo3Cr4V high speed steel. Wear 302:854–862. doi:10.1016/j.wear.2012.12.037
8. D. Das, K.K. Ray, A.K. Dutta. (2008) Influence of temperature of sub-zero treatments on the wear behaviour of die steel. Wear 267:1361-1370. doi:10.1016/j.wear.2008.11.029
9. Junji Li, Xianguo Yan, Xiaoyang Liang et al (2017) Influence of different cryogenic treatments on high-temperature wear behavior of M2 steel. Wear 376-377. doi:10.1016/j.wear.2016.11.041
10. Firouzdor V., Nejati E., Khomamizadeh F.. (2007) Effect of deep cryogenic treatment on wear resistance and tool life of M2 HSS drill. Journal of Materials Processing Technology 206:203-207. doi:10.1016/j.jmatprotec.2007.12.072
11. Yan Xianguo, Pang Siqin, Li Yongtang et al (2009) Electrolytic Strengthening Technology of Cutting Edge of High-Speed Steel Tap. Journal of Mechanical Engineering 45: 203-207.doi:10.3901/JME.2009.04.203
12. Su Haoyang, Zhang Wei, Shen Yuliang et al (2016) Experimental of Electrolytic-abrasive Edge Honing Process for Cemented Carbide Tool. Journal of Tool technology 50: 35-37.
13. C.-F. Wyen, K. Wegener. (2010) Influence of cutting edge radius on cutting forces in machining titanium. CIRP Annals - Manufacturing Technology 59:93-96. doi:10.1016/j.cirp.2010.03.056
14. Wan Qingfeng, Lei Yuyong, Liu Kefu et al (2013) Research on model of tool edge preparation based on micro abrasive water jet. Journal of Modern manufacturing engineering 09: 95-99.

15. Cai Xiao, Pang Guibing, Xin Kaikai et al (2016). Sem analysis of electrochemical corrosion machining on the surface of cement carbide YT15.Journal of the Dalian University of Technology 35: 482-485.
16. Senthilkumar D., Rajendran I., Pellizzari M. et al (2010) Influence of shallow and deep cryogenic treatment on the residual state of stress of 4140 steel. Journal of Materials Processing Technology 211:396-401. doi:10.1016/j.jmatprotec.2010.10.018
17. Yoshinori YAMAOKA, Yoshiaki KAKINO, Tomonori SATO (2002)High Speed and High Productive Tapping by Intelligent Machine Tools (3~(rd) Report).Journal of the Japan Society for Precision Engineering 68:1226-1230.
18. Kou Guofu, Yan Xianguo, Dong Liang et al (2018) Effects of Cryogenic Treatment on Wear Resistance of W6Mo5Cr4V2 High Speed Steel. Journal of Hot Working Process 47:197-200.
19. Kou Guofu, Yan Xianguo, Feng Zhiyang et al (2017) Research on Wear Mechanism of W6M05Cr4V2 High Speed Steel Taps Based on Cryogenic and Passivation Technology. Journal of Tooling technology 51:26-28.
20. Liujie Xu, Jiandong Xing, Shizhong Wei et al (2007) Study on relative wear resistance and wear stability of high-speed steel with high vanadium content. an International Journal on the Science and Technology of Friction 262: 253–261. doi:10.1016/j.wear.2006.05.016
21. Xiangyi Ren, Hanguang Fu, Jiandong Xing et al (2018) Research on high-temperature dry sliding friction wear behavior of CaTi modified high boron high speed steel. Tribology International 132:165-176. doi:10.1016/j.triboint.2018.12.009
22. Chaus A.S., Sitkevich M.V., Pokorný P. et al (2021) Wear resistance and cutting performance of high-speed steel ball nose end mills related to the initial state of tool surface. Wear 472-473. doi:10.1016/J.WEAR.2021.203711
23. Zhi Yang Feng, Xian Guo Yan, Yan Wen Lv. et al (2016) The Effect of Electrolytic Strengthening Treatment on Tap's Service Life. Key Engineering Materials 4283:693-693. doi:10.4028/www.scientific.net/KEM.693.944
24. N.B. Dhokey, J. Dandawate, H. Gangurde et al (2012) Metallurgical investigation of cryogenically cracked M35 tool steel. Engineering Failure Analysis 21:52-58. doi:10.1016/j.engfailanal.2011.11.013
25. Jovičević-Klug Patricia, Jenko Monika, Jovičević-Klug Matic et al (2021) Effect of deep cryogenic treatment on surface chemistry and microstructure of selected high-speed steels. Applied Surface Science. doi:10.1016/J.APSUSC.2021.149257.

Figures

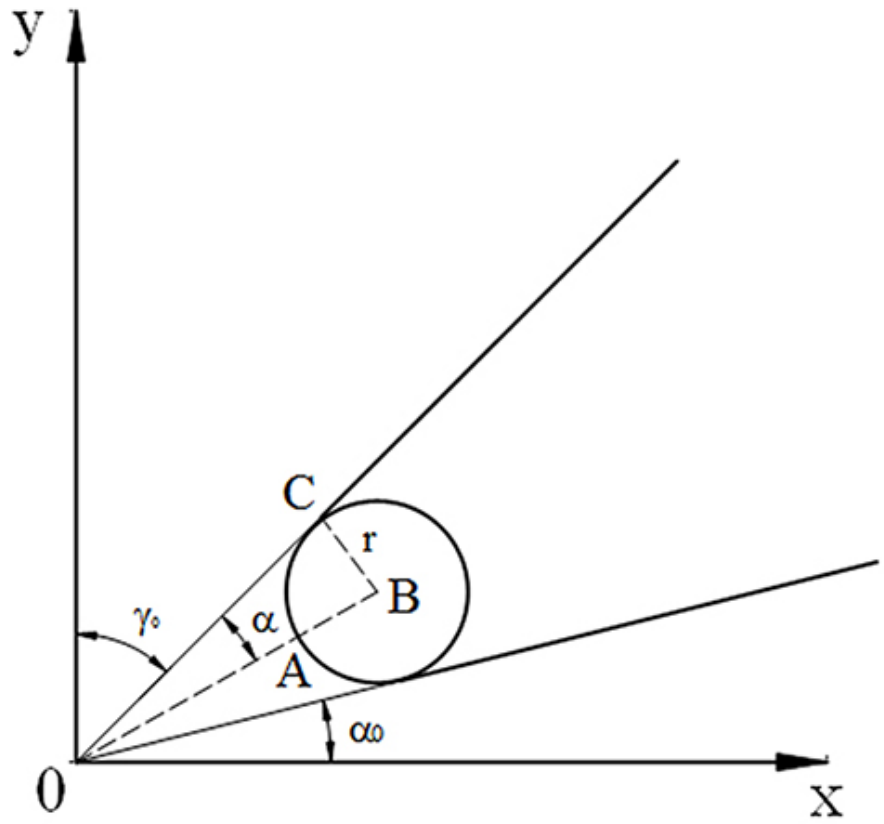

$$\sin\alpha = \frac{BC}{OA + AB} = \frac{r}{r + OA}$$

$$\alpha = \frac{90° - \gamma_0 - \alpha_0}{2}$$

$$\gamma_0 = 8.69°$$

$$\alpha_0 = 4.96°$$

Figure 1

Geometric relation of cutting edge radius of the tool

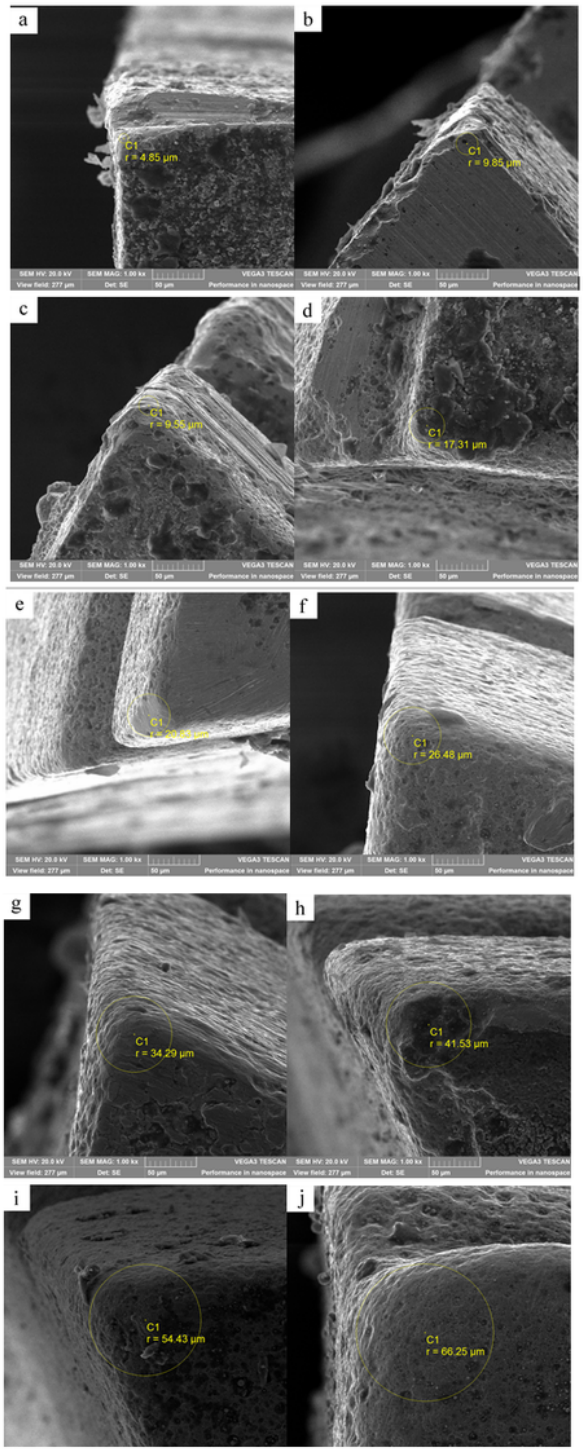

Figure 2

The edge radius of the taps with different charge quantities

a.15C b.30C c.50C d.80C e.100C f. 150C g.200C h.300 i.400C j.500C

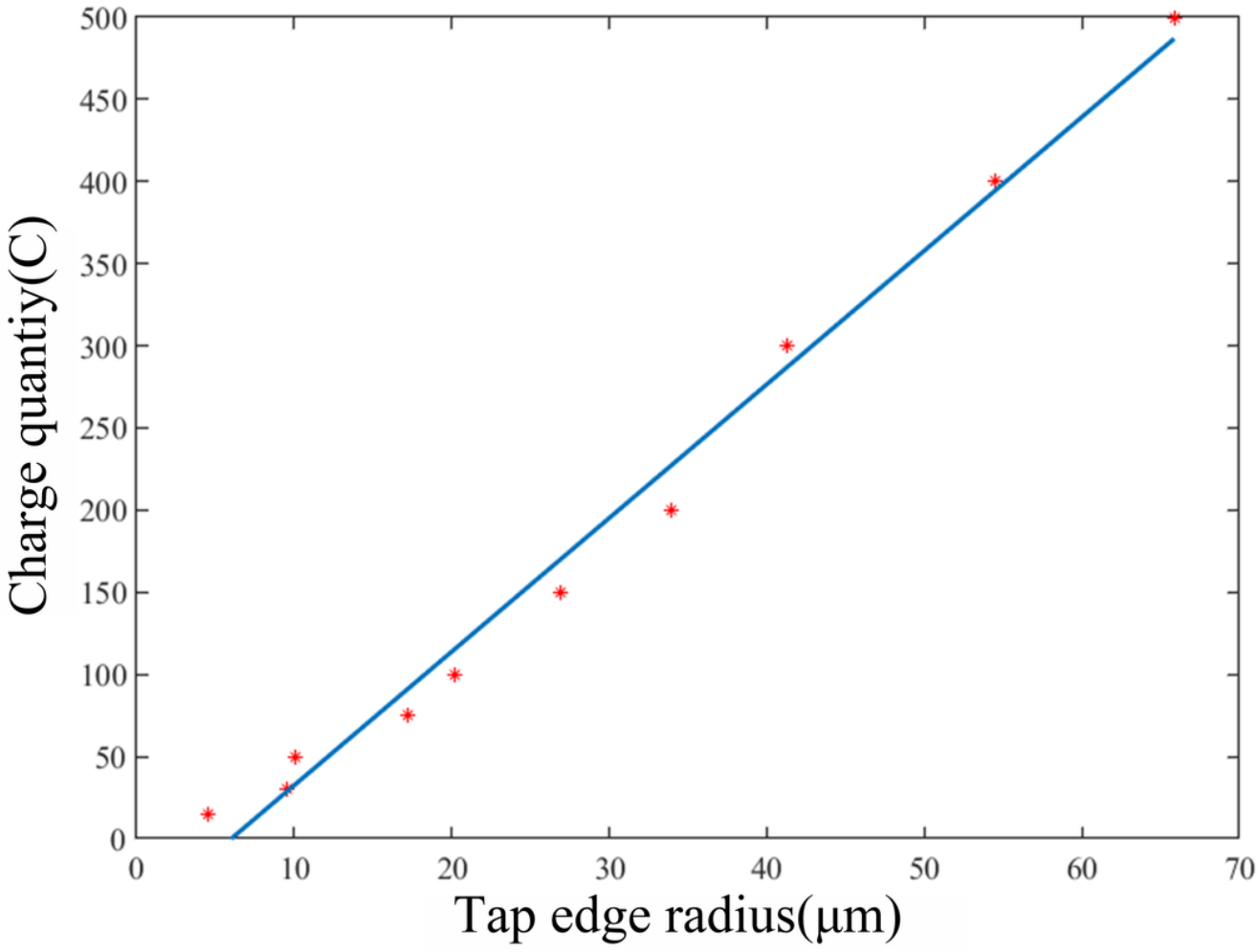

Figure 3

The relationship of the edge radius of the taps with different charge quantities

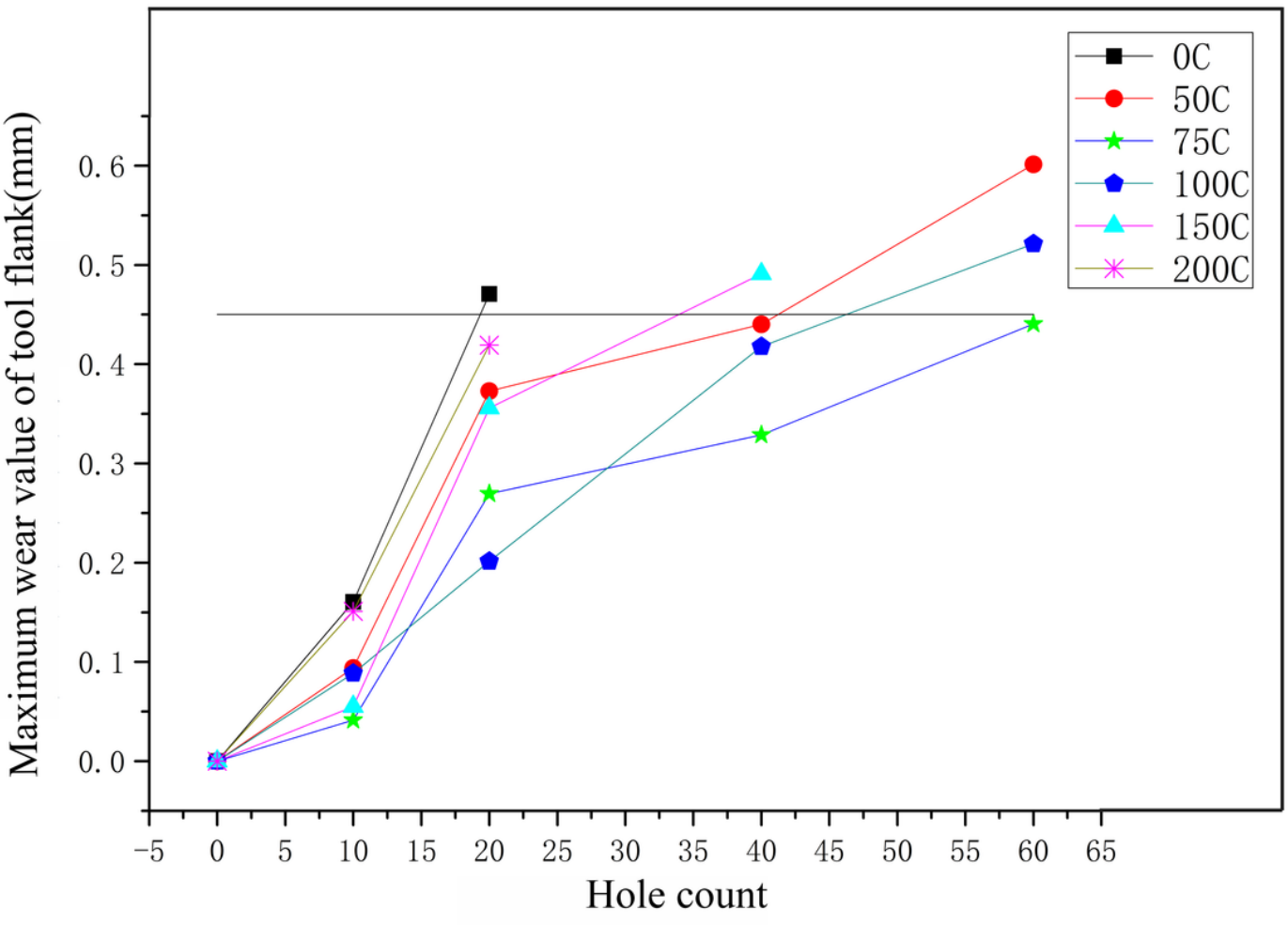

Figure 4

The wear curve of the blade surface after the taps of different electrolytic parameters

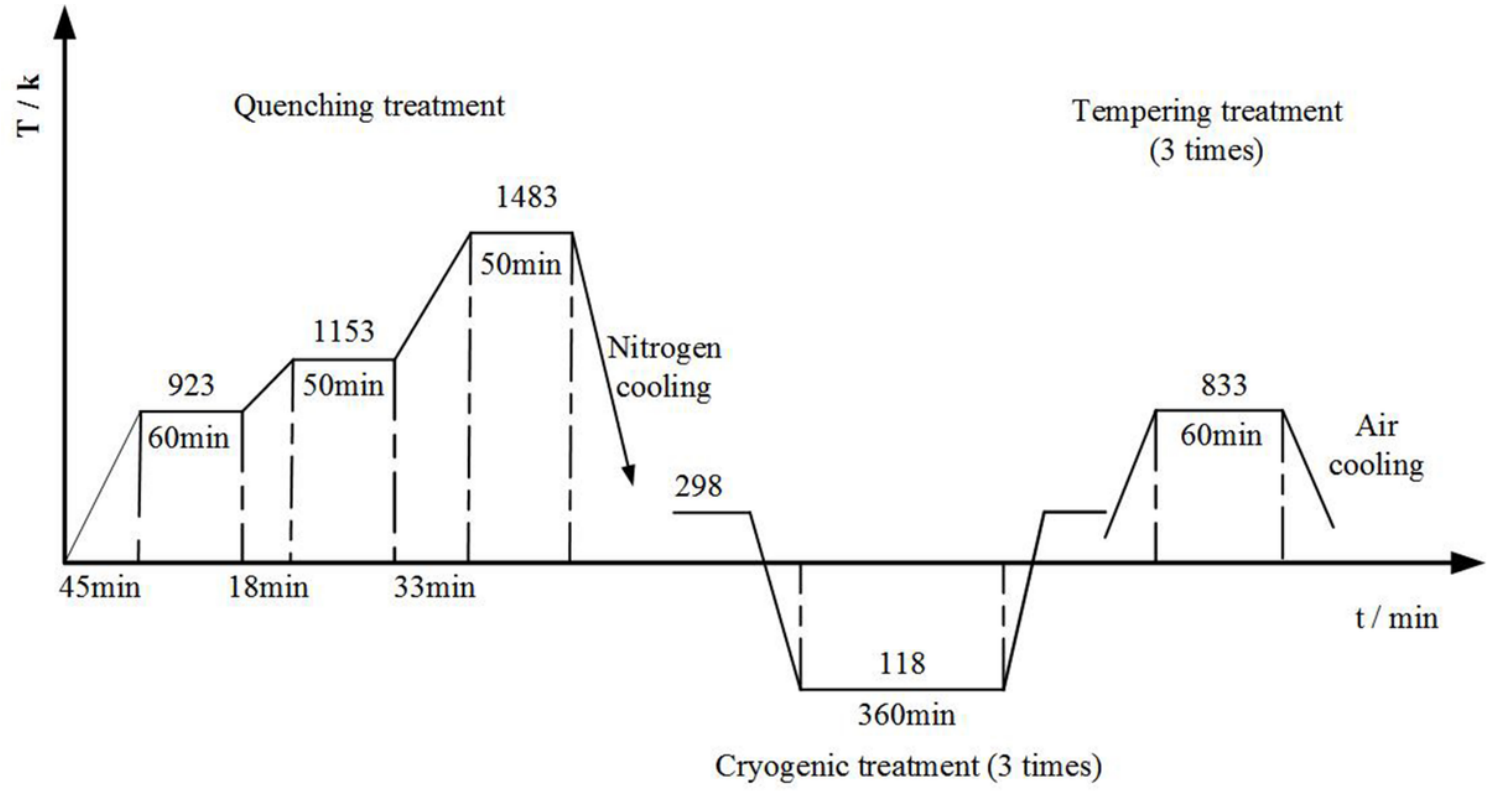

Figure 5

The heat treatment and cryogenic treatment process

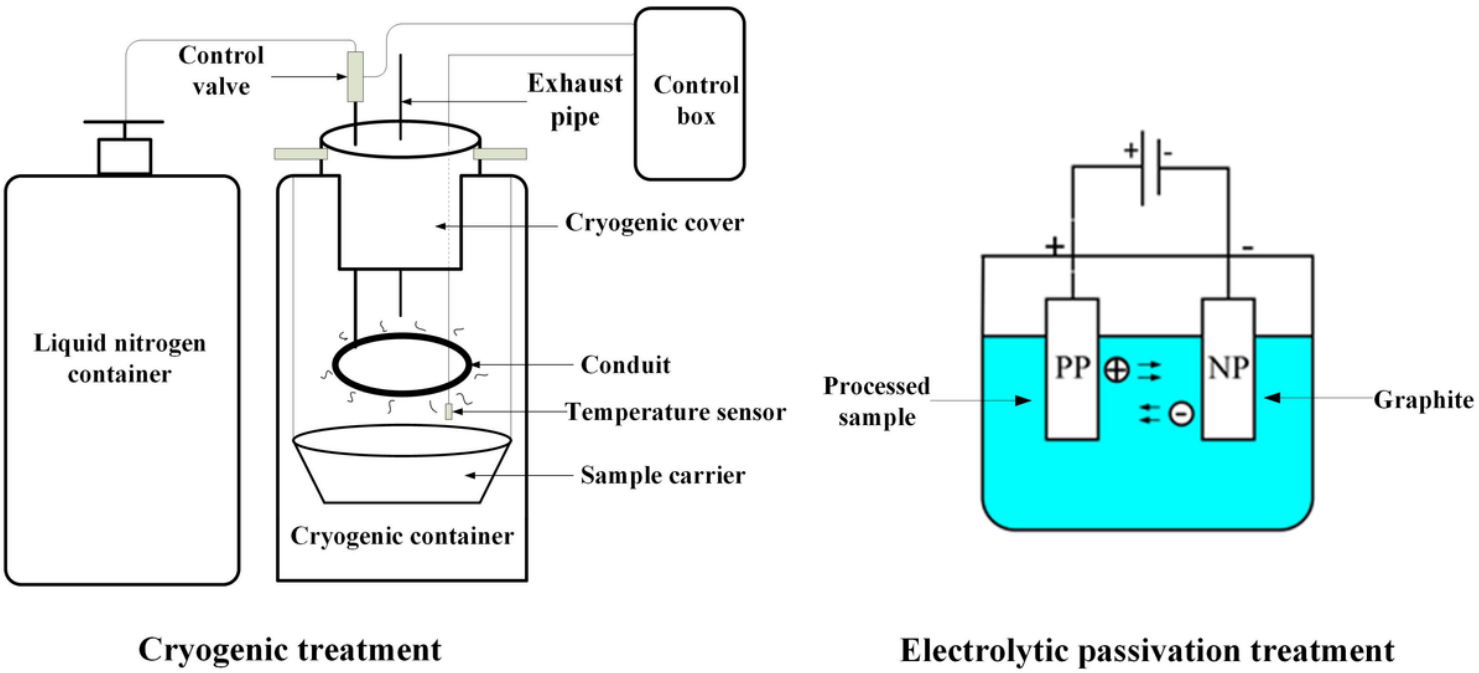

Figure 6

The schematic diagram of cryogenic treatment and electrolytic passivation

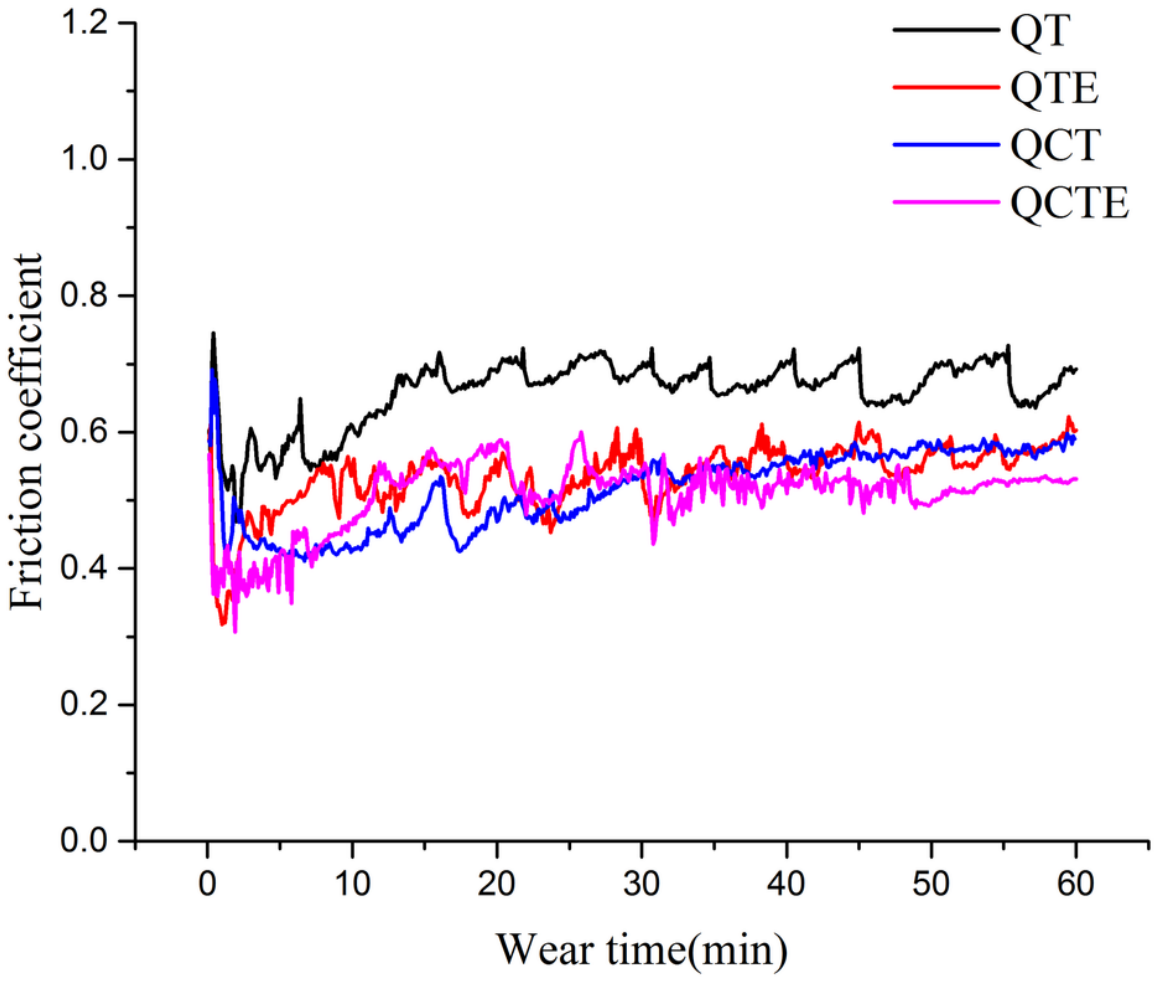

Figure 7

Change of friction coefficient of sample in different processed groups

Figure 8

Morphology of the samples before and after passivation treatment

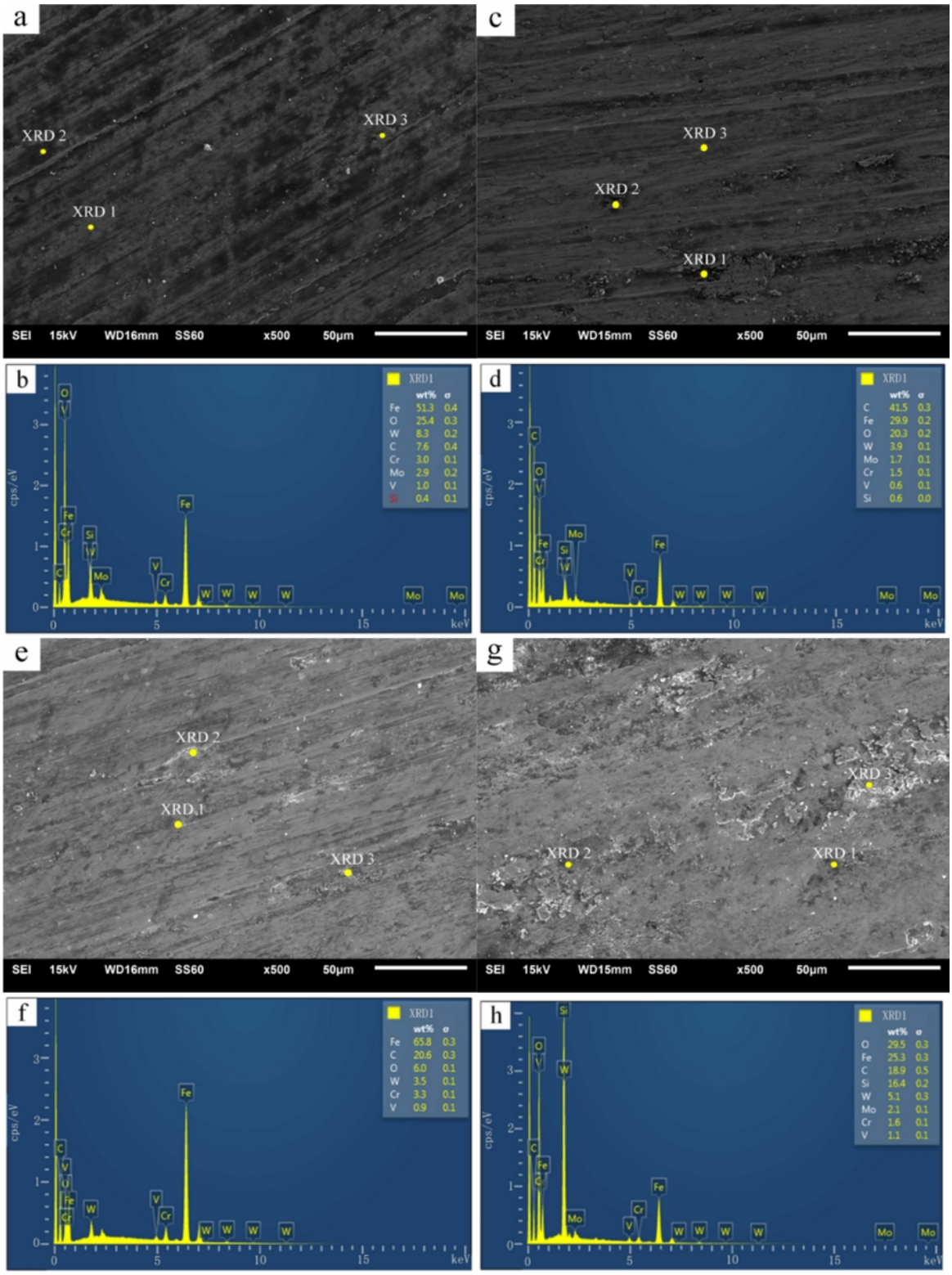

Figure 9

SEM photos of the wear scar of four groups of different processed samples

(a), (b) worn surface morphology and its corresponding EDS spectrum of the QT group samples.

(c),(d) worn surface morphology and its corresponding EDS spectrum of the QCT group samples.

(e),(f) worn surface morphology and its corresponding EDS spectrum of the QTP group samples.

(g),(h) worn surface morphology and its corresponding EDS spectrum of the QCTP group samples.

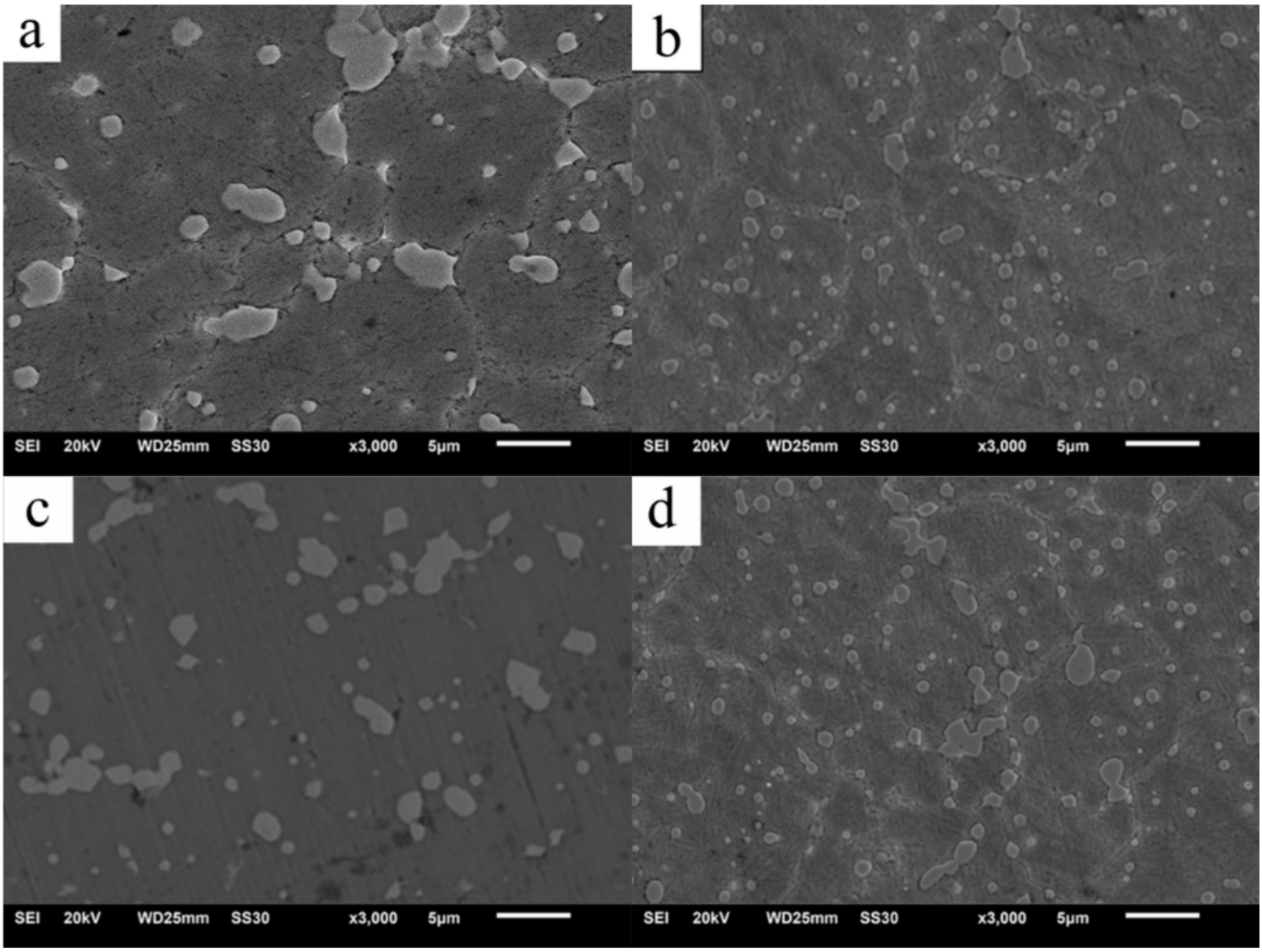

Figure 10

SEM photos of sample microstructure of different treatment process

(a. QT, b. QCT, c. QTP and d. QCTP)